BNL-108003-2015-JA

# *Electronic structure of heavy fermion caged-compound $Ce_3Pd_{20}X_6$ (X = Si, Ge) studied by photoelectron spectroscopy and density functional theory*

Hitoshi Yamaoka,[1,*] Eike F. Schwier,[2,†] Masashi Arita,[2] Kenya Shimada,[2] Naohito Tsujii,[3] Ignace Jarrige,[4] Jian Jiang,[5] Hirokazu Hayashi,[5] Hideaki Iwasawa,[2] Hirofumi Namatame,[2,5] Masaki Taniguchi,[2,5] and Hideaki Kitazawa[3]

[1]RIKEN SPring-8 Center, RIKEN, 1-1-1 Kouto, Sayo, Hyogo 679-5148, Japan
[2]Hiroshima Synchrotron Radiation Center, Hiroshima University, Higashi-Hiroshima, Hiroshima 739-0046, Japan
[3]Quantum Beam Center, National Institute for Materials Science, 1-2-1 Sengen, Tsukuba 305-0047, Japan
[4]National Synchrotron Light Source II, Brookhaven National Laboratory, Upton NY 11973, USA
[5]Graduate School of Science, Hiroshima University, Higashi-Hiroshima, Hiroshima 739-0046, Japan

*Submitted to Physical Review B*

March 2015

**NSLS II, Photon Science Division**

**Brookhaven National Laboratory**

**U.S. Department of Energy**
**DOE – Office of Science**

Notice: This manuscript has been co-authored by employees of Brookhaven Science Associates, LLC under Contract No. DE-SC0012704 with the U.S. Department of Energy. The publisher by accepting the manuscript for publication acknowledges that the United States Government retains a non-exclusive, paid-up, irrevocable, world-wide license to publish or reproduce the published form of this manuscript, or allow others to do so, for United States Government purposes.

# DISCLAIMER

This report was prepared as an account of work sponsored by an agency of the United States Government. Neither the United States Government nor any agency thereof, nor any of their employees, nor any of their contractors, subcontractors, or their employees, makes any warranty, express or implied, or assumes any legal liability or responsibility for the accuracy, completeness, or any third party's use or the results of such use of any information, apparatus, product, or process disclosed, or represents that its use would not infringe privately owned rights. Reference herein to any specific commercial product, process, or service by trade name, trademark, manufacturer, or otherwise, does not necessarily constitute or imply its endorsement, recommendation, or favoring by the United States Government or any agency thereof or its contractors or subcontractors. The views and opinions of authors expressed herein do not necessarily state or reflect those of the United States Government or any agency thereof.

# Electronic structure of heavy fermion caged-compound $Ce_3Pd_{20}X_6$ ($X$ = Si, Ge) studied by photoelectron spectroscopy and density functional theory

Hitoshi Yamaoka,[1,*] Eike F. Schwier,[2,†] Masashi Arita,[2] Kenya Shimada,[2] Naohito Tsujii,[3] Ignace Jarrige,[4] Jian Jiang,[5] Hirokazu Hayashi,[5] Hideaki Iwasawa,[2] Hirofumi Namatame,[2,5] Masaki Taniguchi,[2,5] and Hideaki Kitazawa[3]

[1] *RIKEN SPring-8 Center, RIKEN, 1-1-1 Kouto, Sayo, Hyogo 679-5148, Japan*
[2] *Hiroshima Synchrotron Radiation Center, Hiroshima University, Higashi-Hiroshima, Hiroshima 739-0046, Japan*
[3] *Quantum Beam Center, National Institute for Materials Science, 1-2-1 Sengen, Tsukuba 305-0047, Japan*
[4] *National Synchrotron Light Source II, Brookhaven National Laboratory, Upton New York 11973, USA*
[5] *Graduate School of Science, Hiroshima University, Higashi-Hiroshima, Hiroshima 739-0046, Japan*

(Dated: October 23, 2014)

The electronic structure of $Ce_3Pd_{20}X_6$ ($X$ = Si, Ge) has been studied by using detailed density functional theory (DFT) calculations and high-resolution photoelectron spectroscopy (PES) measurements. The orbital decomposition of the electronic structure by DFT calculations indicate that the Ce atoms in the (8c) site surrounded by 16 Pd atoms have a more localized nature and a tendency to be magnetic. Ce atoms in the (4a) site surrounded by 12 Pd and 6 $X$ atoms, on the other hand, show only a negligible magnetic moment. In the photoemission valence-band spectra we observe a strong $f^0$ ($Ce^{4+}$) component with a small fraction of $f^1$ ($Ce^{3+}$) component. The spectral weight of the $f^1$ component near the Fermi level of $Ce_3Pd_{20}Si_6$ is stronger than that for $Ce_3Pd_{20}Ge_6$ at the $4d$-$4f$ resonance, suggesting stronger $c$-$f$ hybridization in the former. This may hint to the origin of the large electronic specific coefficient of $Ce_3Pd_{20}Si_6$ compared to $Ce_3Pd_{20}Ge_6$.

## I. INTRODUCTION

The caged compound $Ce_3Pd_{20}Si_6$ is known to be one of the heaviest electron Kondo systems with a low-temperature electronic specific heat coefficient of $\gamma = 8$ J/mol K$^2$.[1,2] Such large $\gamma$ value is normally attributed to strong electron correlations and a large density of states (DOS) at the Fermi level ($E_F$). $Ce_3Pd_{20}Si_6$ has a characteristic geometric structure: Pd and Si atoms form cages which accommodate Ce guest ions. The family of $R_3Pd_{20}X_6$ ($R$ = La, Ce; $X$ = Si, Ge) compounds is a potential candidate for thermoelectric applications, having large thermoelectric figure of merit, which is derived from the rattling motion of guest atoms in the cage structure.[3–8] Furthermore, it has attracted much interest that the quantum criticality might be achieved in $Ce_3Pd_{20}Si_6$ by hydrostatic pressure, chemical pressure, and magnetic field.[9]

In $Ce_3Pd_{20}Si_6$ Ce atoms occupy two different crystallographic sites of 8c and 4a, which are surrounded by 16 Pd atoms and 12 Pd and 6 Si atoms, respectively.[10] With decreasing temperature a quadrupole order at $T_Q = 0.52$ K at the (8c) site[11] and antiferromagnetic order at $T_N = 0.33$ K at the (4a) site[12] occurred and both orders coexist at low temperature. Temperature dependence of the resistivity showed a typical behavior due to incoherent Kondo scattering.[1,5] Its maximum corresponds to the onset of the Kondo screening at the Kondo temperature $T_K \approx 20$ K. It was suggested that Ce on the (4a) site determined the Kondo properties, while Ce on the (8c) site is responsible for the unusual magnetic behavior.[13,14] Magnetic susceptibility was Curie-Weiss like above 100 K with an effective magnetic moment close to the theoretical value of $2.54\mu_B$ based on the Hund rule.[1] Therefore Ce in the cage was expected to be nearly in a $Ce^{3+}$ state at high temperature. All this resulted in a complex magnetic phase diagram.[11,12,15,16] Under a magnetic field the resistivity showed a linear temperature dependence in the range between 0.1-0.6 K.[4] This non-Fermi liquid behavior signaled a field-induced quantum critical point.[3,6,17] Thus $Ce_3Pd_{20}Si_6$ underwent a quantum phase transition triggering the Kondo breakdown, under the magnetic field with decreasing $T_N$ and increasing $T_Q$.[18] The pressure effect on the transport properties was also studied, showing characteristic features of these Kondo compounds for the Hall constant and the electrical resistivity.[19] However, the specific heat showed little pressure dependence. To explain the contrasting behavior, two Kondo temperatures for each Ce site were considered. The Crystal Field (CF) effect is also important to understand the magnetic properties. Neutron diffraction[20] and ultrasonic measurements[11] showed a $\Gamma_7$ quartet ground state for the (4a) site, and $\Gamma_8$ for the (8c) site. However, the extrapolation from the inelastic neutron scattering showed the CF ground-state at both Ce sites ((8c) and (4a)) to be the $\Gamma_8$ quartet.[21]

On the other hand, the isostructural germanide compound $Ce_3Pd_{20}Ge_6$ is a heavy-electron system with a Kondo temperature of a few K.[2] The electronic specific heat coefficient of $\gamma \sim 0.7$ J/mol K$^2$ was smaller by one order of magnitude compared to that of $Ce_3Pd_{20}Si_6$ and the effective moment is nearly equal to that of free trivalent $Ce^{3+}$.[2] and therefor comparable to that in $Ce_3Pd_{20}Si_6$. In $Ce_3Pd_{20}Ge_6$ similar to $Ce_3Pd_{20}Si_6$, $T_Q = 1.2$ K and $T_N = 0.75$ K were reported.[22] A $\mu$SR study indicated that Ce ions at the (4a) site played a major role in Kondo-like behavior[23] similar to $Ce_3Pd_{20}Si_6$. Local density approximation (LDA) calculation for $La_3Pd_{20}Ge_6$ including relativistic effect with the spin-orbit interaction showed stronger mixing effects at the (4a) site than compared to the (8a) site.[24] Under pressure $T_N$ and $T_Q$

did not change up to 0.3 GPa.[25] Ultrasonic experiment showed an off-center rattling motion of $\Gamma_5$ type at the (4a) site.[26] Thermally activated rattling of the Ce ion over an anharmonic potential in a cage was observed for the Ge compound, but not for the Si system.[26,27] For $Ce_3Pd_{20}X_6$ ($X$ = Si, Ge) no photoelectron spectroscopy nor density functional theory (DFT) studies of the electronic structure have been reported so far.

In this paper we report results of DFT calculations as well as ultraviolet (UV) and soft x-ray (SX) photoelectron spectroscopy measurements[28,29] for $Ce_3Pd_{20}X_6$ ($X$ = Si, Ge). We present calculations of the electronic states of both compounds and discuss the site and spin resolved nature of the Pd and Ce contributions to the electronic structure. We further analyze the $k$- and orbital weight dependent band structure at $E_F$ in order to probe the presence of $c$-$f$ hybridization as well as specific differences between both compounds. We then describe the temperature dependence of the valence band in the wide energy range and near $E_F$. Results from $4d$-$4f$ resonant PES in the SX energy range are also presented and Ce $4f$ derived spectra will be discussed.

## II. DENSITY FUNCTIONAL THEORY CALCULATIONS

### A. Crystal structure

In Fig. 1 we show a schematic image of the cubic $Cr_{22}C_6$-type crystal structure (space group $Fm\bar{3}$m, No. 225) of $Ce_3Pd_{20}Si_6$ and $Ce_3Pd_{20}Ge_6$.[10] The simple unit cell contains 116 atoms, consisting of 12 Ce, 80 Pd and 24 $X$ = (Si, Ge) atoms. In the primitive unit cell the number of nonequivalent atoms is reduced to 2 $Ce_{8c}$, 1 $Ce_{4a}$, 12 $Pd_{mix}$, 8 $Pd_{8c}$ as well as 6 $X$ = (Si, Ge) atoms. While the fractional coordinates in both unit cells are identical, the lattice constants of $Ce_3Pd_{20}Ge_6$ are expanded by ∼1.3 % compared to $Ce_3Pd_{20}Si_6$.[10,21,22]

As mentioned above, Ce atoms occupy two different crystallographic sites (8c) and (4a) in the crystal structure. The two $Ce_{8c}$ atoms on the (8c) site, with cubic $T_d$ symmetry, are located inside a cage made up of 16 Pd atoms. These Pd atoms are classified into 4 $Pd_{8c}$ atoms which tetrahedrally surround the $Ce_{8c}$ atoms with a shorter bond length and 12 $Pd_{mix}$ atoms with a slightly longer distance from the $Ce_{8c}$. The $Pd_{16}$ cages form a simple cubic sublattice inside the crystal. The $Ce_{4a}$ atom on the (4a) site with cubic $O_h$ symmetry is surrounded by a cage consisting of 12 $Pd_{mix}$ and 6 $X$ = (Si, Ge) atoms in a face-centered cubic sublattice. Each of the 12 $Pd_{mix}$ atoms in the unit cell is part of three Ce cages, sharing a bond with two neighboring $Ce_{8c}$ and one neighboring $Ce_{4a}$ atoms. The bond length with the latter is shorter suggesting a stronger interaction between the $Pd_{mix}$ atoms and the Ce at the (4a) site compared to the (8c) site. We may assume that the electronic states of $Pd_{8c}$ atoms with the shortest Ce-Pd bond length in the system are well localized within the $Ce_{8c}$ cage.

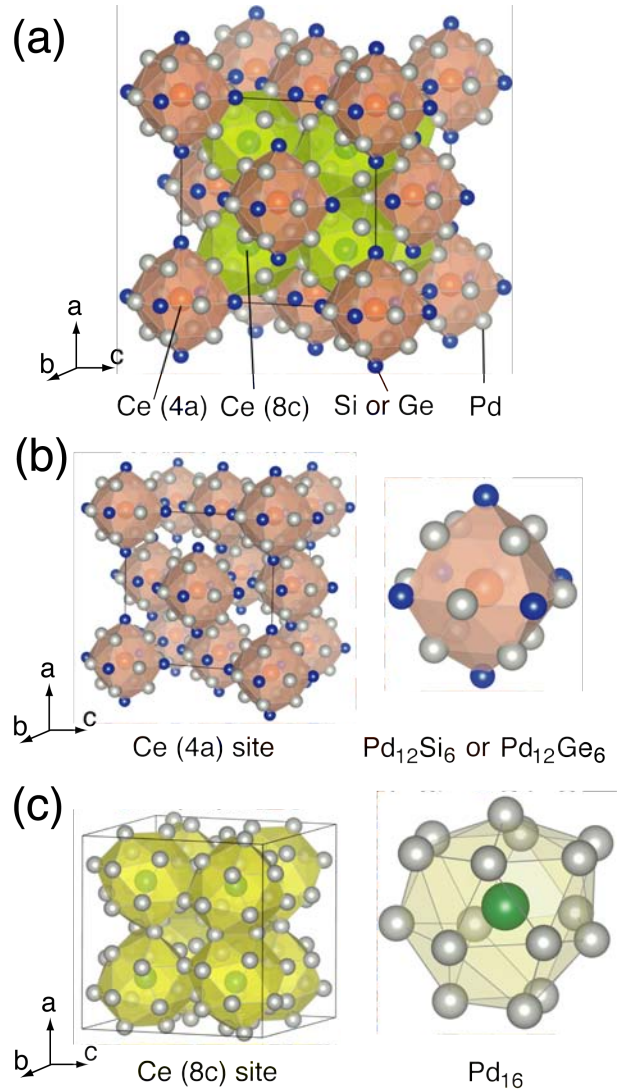


FIG. 1. (Color online). (a) Schematic image of the cubic $Cr_{22}C_6$-type crystal structure of $Ce_3Pd_{20}X_6$ ($X$ = Si, Ge). (b) $Ce_{4a}$ on site (4a) is surrounded by a cage of 12 $Pd_{mix}$ and 6 Si/Ge atoms. (c) $Ce_{8c}$ on site (8c) is inside a cage of 4 $Pd_{8c}$ and 12 $Pd_{8c}$ atoms.

### B. Partial Density of States

Taking into account the above crystal structures we performed fully relativistic DFT calculations for $Ce_3Pd_{20}X_6$ ($X$ = Si, Ge) using the *elk* code,[30] which is based on an all-electron full-potential linear augmented plane wave (FP-LAPW) method. Exchange and correlation energies were described by the LSDA functional introduced by Perdew and Wang[31] and we used a $4 \times 4 \times 4$ Mankhorst-Pack mesh[32] centered around the L-point leading to 32 nonequivalent $k$-points sampling the Bril-

louin zone. The maximum cutoff energy was 450 eV. In the beginning of the self-consistent cycle a magnetic field was applied throughout the entire unit cell in order to break spin symmetry and allow the magnetic ground state to emerge.[33]

In Fig. 2 we compare the spin and site integrated contributions to the DOS of $Ce_3Pd_{20}Si_6$ (2(a)-2(d)) and $Ce_3Pd_{20}Ge_6$ (2(e)-2(h)). In the topmost two graphs (2(a) and 2(e)) we highlight the main contributions from each species to the DOS, namely the Ce $f$, Pd $d$ and $X$ = (Si, Ge) $p$ orbitals. In the three graphs below we have resolved the contributions of all orbitals ($s, p, d$, and $f$) from the three species inside the unit cell of $Ce_3Pd_{20}Si_6$ (2(b)-2(d)) and $Ce_3Pd_{20}Ge_6$ (2(f)-2(h)).

The first thing to notice is the overall close resemblance of the DOS of $Ce_3Pd_{20}Si_6$ and $Ce_3Pd_{20}Ge_6$ as well as the overall weak contribution from $X$ = (Si, Ge) orbitals to the electronic structure. The Ce $f$ states are the main contribution to the conduction band and the valence band is dominated by Pd $d$ electrons with some contribution of $X$ $p$ electrons at higher binding energies. At the Fermi edge there is a weak multipeak structure in the Ce $4f$ density mixing with Pd $d$ states (Figs. 2(b) and 2(f), inset). The contribution from the $4f$ states is also clearly demonstrated by the Ce $4d - 4f$ resonance during the PES measurements.

Searching for differences between the DOS of $Ce_3Pd_{20}Si_6$ and $Ce_3Pd_{20}Ge_6$ we find a small shift ($\sim$ 30 meV) of the valence-band maximum ($E_{\rm b} \sim 1.3$ eV, where $E_{\rm b}$ is the binding energy) towards $E_{\rm F}$. The main features inside the valence band exhibit a more significant shift ($\sim$ 220 meV) in the same direction. The conduction band as a whole also exhibits a small shift of $\sim$ 30 meV, again towards $E_{\rm F}$.

While the overall DOS exhibits only minor differences between $Ce_3Pd_{20}Si_6$ and $Ce_3Pd_{20}Ge_6$, the literature shows very pronounced changes between the properties of the two compounds, the electric specific heat $\gamma_{exp}$ being one example. This apparent mismatch between theory and experiment may be taken as a signature of correlation effects being present in these compounds.

Generally speaking, it is possible to derive the electric specific heat $\gamma_{theo}$ ($= \frac{2}{3}\pi^2 {k_B}^2 \rho(E_{\rm F})$) from the calculated density of states at the Fermi level $\rho(E_{\rm F})$. If we define the enhancement factor $\widetilde{\gamma} = \gamma_{exp}/\gamma_{theo}$ as a measure of the correlation strength in a material we can use $\rho(E_{\rm F})$ for $Ce_3Pd_{20}Si_6$ (13 states/eV/unit cell) and $Ce_3Pd_{20}Ge_6$ (17.5 states/eV/unit cell) to derive $\widetilde{\gamma}_{\rm CPS} \sim 250$ for $Ce_3Pd_{20}Si_6$ and $\widetilde{\gamma}_{\rm CPG} \sim 30$ for $Ce_3Pd_{20}Ge_6$. This result suggests that even though the experimental value of the electronic specific heat of $Ce_3Pd_{20}Ge_6$ is about one order of magnitude lower than that of $Ce_3Pd_{20}Si_6$ both materials are actually strongly correlated.

The values of $\rho(E_{\rm F})$ of both compounds also suggests that differences between the two may be present on a smaller energy scale close to the Fermi level even though the overall DOS is comparable. The difference of $\widetilde{\gamma}$, on the other hand, provided an indication that renormalized

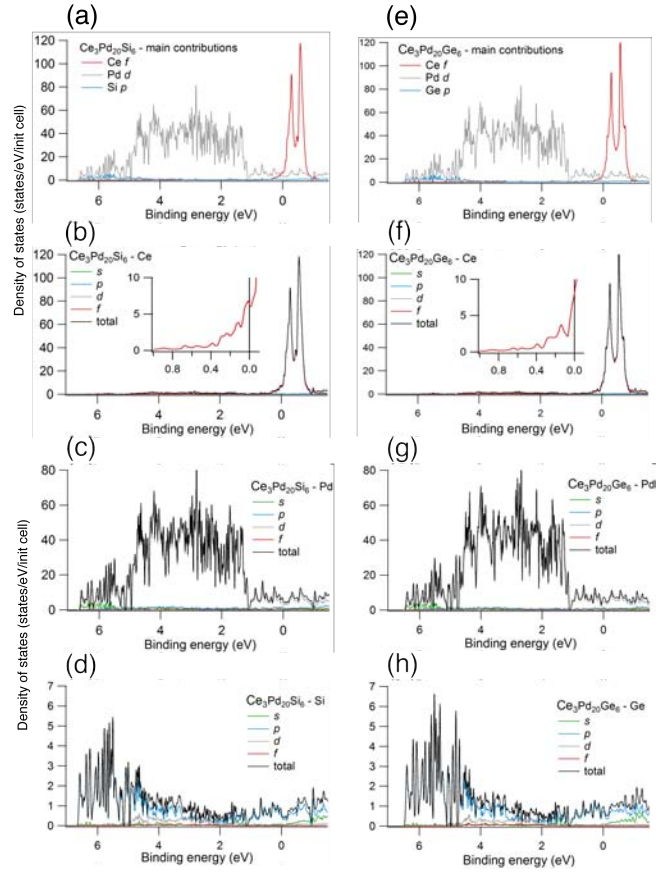


FIG. 2. (Color online). (a) Main contributions to the density of state of $Ce_3Pd_{20}Si_6$ (CPS) from Ce $f$, Pd $d$ and Si $p$ orbitals. (b)-(d) Partial density of states calculated within density functional theory for each species in $Ce_3Pd_{20}Si_6$. (e) Main contributions to the density of state of $Ce_3Pd_{20}Ge_6$ (CPG) from Ce $f$, Pd $d$ and Ge $p$ orbitals. (f)-(h) Partial density of states calculated within density functional theory for each species in $Ce_3Pd_{20}Ge_6$.

Ce $f$ electrons should be considered to drive properties of a correlated ground state. While more advanced theoretical methods are necessary to discuss the correlated nature of the Ce $4f$ electrons, we may still use our DFT results to shine some light on the spectra in the experimental section. We will also try to highlight more of the less pronounced differences between $Ce_3Pd_{20}Si_6$ and $Ce_3Pd_{20}Ge_6$ as well as between the Ce 8c/4a and Pd mix/8c sites which may facilitate our understanding on the physical properties of these compounds

### C. Spin and Site resolved DOS

In Fig. 3, we plot spin and site resolved DOS of the $Pd_{8c}$ and $Pd_{mix}$ (Fig. 3(a)) and the $Ce_{8c}$ and $Ce_{4a}$ (Fig. 3(b)) sites for $Ce_3Pd_{20}Si_6$.[34] Due to the overall similarity of the DOS as seen in Fig. 2, we omit plotting the corresponding graphs for $Ce_3Pd_{20}Ge_6$.

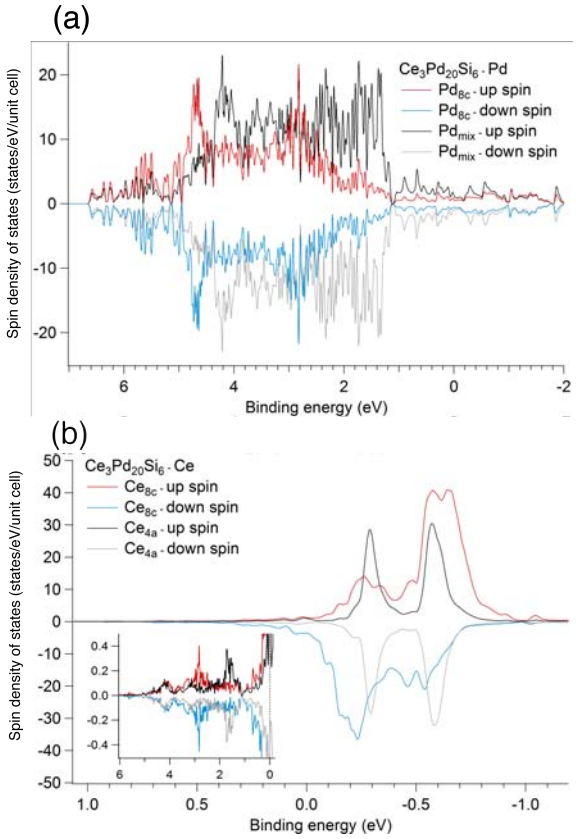


FIG. 3. (Color online). (a) Spin and site resolved Pd $d$ partial density of states for $Ce_3Pd_{20}Si_6$. (b) Spin and site resolved Ce $f$ partial density of states for $Ce_3Pd_{20}Si_6$.

In Fig. 3(a) we see that $Pd_{mix}$ dominates the low binding energy region of the valence band between $E_b = 1.2$ and 2.3 eV and has a peak at $E_b = 4.1$ eV. The $Pd_{8c}$ states contribute to the valence band around $E_b = 2.8$ eV and $E_b = 4.7$ eV. Both species contribute states around $E_b = 5.6$ eV where the Si $p$ states are mainly localized (see Fig. 2(d)). Neither Pd site exhibits any spin polarization in the valence band, which is in accordance with the results from the calculation of the magnetic moment at the Pd atoms, which showed only a negligible moment.

As $Pd_{8c}$ is at least partially shared between one (4a) and two (8c) cages we may speculate that they facilitate an interaction between the different Cerium sites. The more delocalized character of these atoms is also supported by the fact that their partial DOS is slightly increased in the $c$-$f$ hybridization region close to $E_F$ (Fig. 3(a)).

It has been suggested that each Ce site plays a specific role in determining the Kondo (4a) and magnetic (8c) properties of these materials. And indeed we find that the calculation predicts a magnetic moment and a slightly higher valency for $Ce_{8c}$ compared to $Ce_{4a}$.

These differences are mirrored in the density of states, if we compare the bandwidth and spin polarization of the conduction bands of $Ce_{8c}$ and $Ce_{4a}$ (Fig. 3(b)). We see that the (8c) coordination in the $Pd_{16}$ cage leads to a larger band width i.e. less electronic localization and a strong spin polarization in the unoccupied states. Both can be seen to lead to a dominance of spin polarized $f$ states from the (8c) site at and below $E_F$ (Fig. 3(b) and inset). Taking into account the total number of $Ce_{8c}$ atoms per unit cell, the contribution at and below $E_F$ (i.e. the $c$-$f$ hybridization region) is more than twice as large as the corresponding $Ce_{4a}$ weight. One the other hand, the $f$ states from $Ce_{4a}$ show no significant magnetic polarization in the conduction band, a much smaller band width and only limited polarization in the $c$-$f$ region. These results are consistent with the $\mu$SR study[23] for $Ce_3Pd_{20}Ge_6$ and the LDA calculation[24] for $La_3Pd_{20}Ge_6$.

Interestingly, additional $f$ states, even though very low in density, from both Ce sites are present in the valence band (Fig. 3(b), inset) below the $c$-$f$ region. The $Ce_{8c}$ from the $Pd_{16}$ cage contributes additional $f$ states around $E_b = 2.8$ eV. While the mixed cage $Ce_{4a}$ site adds $f$ weight around $E_b = 1.7$ and 3.1 eV to the valence band and around $E_b = 4.2$ eV close to the bottom of the valence band. However, in contrast to the conduction band and the $c$-$f$ region, neither of the $f$ states in the valence band are spin polarized, most likely due to the dominant weight of the Pd $d$ electrons.

### D. Spectral weight in the $c$-$f$ hybridization close to the Fermi level

In Fig. 4 we have plotted the $Ce_{8c}$ $f$ (a) and $Pd_{8c}$ $d$ (b) weighted band structure of the $Pd_{16}$ cage as well as the $Ce_{4a}$ $f$ (c) and $Pd_{mix}$ $d$ (d) weighted band structure of the $Pd_{12}Si_6$ cage.[35] Starting with the $Pd_{16}$ cage (Figs. 4(a) and 4(b)), thought to be responsible for the magnetic properties, we see the contribution from the spin polarized $f$ electrons in the conduction band above $E_b = -100$ meV decaying into the $c$-$f$ region. The $f$ weight is comparable at different $k$-points in the Brillouin zone and is reduced with increasing binding energy. The $Pd_{8c}$ $d$-weight on the other hand is strongly reduced in the hole like bands at the Γ-point as well as several bands at higher binding energy near the Γ- and L-points.

The $f$ and $d$ weighted band structure contributed by the $Pd_{12}Si_6$ cage, thought to be responsible for the Kondo properties, exhibits some particular differences compared to the corresponding $Pd_{16}$ cage plots. First we see the more localized nature of the conduction band indicated by its lower binding energy onset above $E_b = -200$ meV. In the $c$-$f$ region the $f$ weight is strongly localized in the hole pocket at the Γ-point, weakly around the L-points and almost completely absent below the Fermi level at the other high symmetry points. Contrarily, the $Pd_{mix}$ $d$-weight is more homogeneously distributed across the Brillouin zone, compared to the $Pd_{8c}$ $d$-weight. In particular we now see a strong contribution at the Γ-point and around the L-point, but also a slight increase of the $d$-

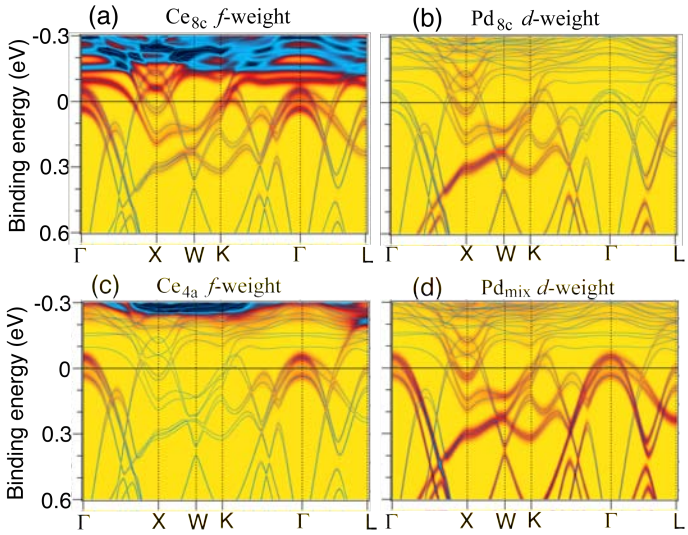


FIG. 4. (Color online). (a) Band dispersion in the $c$-$f$ hybridization of $Ce_3Pd_{20}Si_6$ weighted by the $Ce_{8c}$-$f$ states. (b) $Pd_{8c}$-$d$ states (c) $Ce_{4a}$-$f$ states (d) $Pd_{mix}$-$d$ states

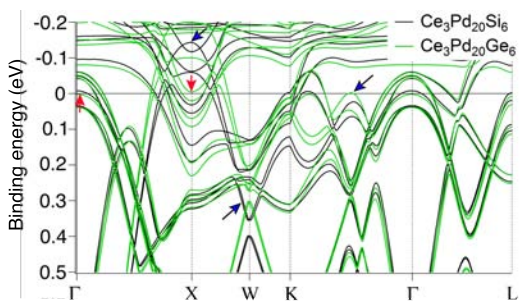


FIG. 5. (Color online). Band dispersion in the $c$-$f$ hybridization of $Ce_3Pd_{20}Si_6$ (black) and $Ce_3Pd_{20}Ge_6$ (green). Red arrows mark the grazing bands $Ce_3Pd_{20}Ge_6$. Blue arrow mark regions with increased energy shift between both compounds.

weight in the bands at the X-point compared to $Pd_{8c}$. As mentioned during the initial discussion, the $Pd_{8c}$ atoms are strongly bound to the $Ce_{8c}$ and we have reasoned that $Pd_{mix}$ may be more hybridized with the Ce at the (4c) site due to the reduced bond length. This is now being validated by the fact that the $Pd_{mix}$ weight is more equally distributed across the Brillouin zone compared to $Pd_{8c}$.

### E. Comparison of the bare band structures of both compounds

In Fig. 5 we compare the unweighted band structure of $Ce_3Pd_{20}Si_6$ and $Ce_3Pd_{20}Ge_6$ at the same high symmetry points used in the previous section. In both calculations 6 bands are crossing the Fermi level. However, for $Ce_3Pd_{20}Si_6$ 4 of these 6 form hole pockets around the Γ-point and 2 electron like pockets at the X-point. While $Ce_3Pd_{20}Ge_6$ has 3 Fermi level crossings of hole like bands at the Γ-point and 3 crossings of electron like bands around the X-point. The dominance of hole pockets in $Ce_3Pd_{20}Si_6$ compared to $Ce_3Pd_{20}Ge_6$ should lead to a change in the nature of the charge carriers between both systems.

Furthermore, in the case of $Ce_3Pd_{20}Ge_6$ one additional hole like band at the Γ-point and one additional electron like band at the X-point graze the Fermi level within 2 and 5 meV, respectively (red arrows). These energy differences are below the precision of our present calculation and at the current state it is not possible to argue if one of these bands may be crossing the Fermi level. In the latter case at least one more band would be contributing to the Fermi surface of $Ce_3Pd_{20}Ge_6$ compared to $Ce_3Pd_{20}Si_6$. However, even if the Fermi level were to lie in the gap between both bands, such small energy gaps can be expected to be overcome by temperature activated excitation of electrons or holes, if the system is at temperatures of a few K.[36] This would lead to two more bands contributing to the conducting properties of $Ce_3Pd_{20}Ge_6$ and strongly effect the temperature dependent properties of the material.

Apart from the number of bands crossing the Fermi level, it is possible to compare the relative energy shifts of corresponding bands between both compounds due to the overall similarities in the band structure. The majority of bands close to the Fermi level is shifted between 0 and several 10 meV to higher binding energies, if $Ce_3Pd_{20}Si_6$ is compared to $Ce_3Pd_{20}Ge_6$. That alone may be explained by a quasi-rigid band shift of the Fermi level or the under-sampling of the differently sized Brillouin zones. There are, however, notable exceptions from this behavior where we find a shift of up to 120 meV in the opposite direction at the X-, W- and K-points and more importantly along the $\overline{K\Gamma}$ line (blue arrows). Along this high symmetry line we see that the topmost hole-like band visible at the Γ-point in $Ce_3Pd_{20}Ge_6$ cross the Fermi level again as a hole pocket around the center of the $\overline{K\Gamma}$ line, while the corresponding band in $Ce_3Pd_{20}Si_6$ remains well below $E_F$.

Even though at the current stage it it not possible to resolve the band structure of either compounds experimentally, these theoretical results may motivate future Hall, de Haas-van Alphen or angle resolved photoemission experiments that should be able to probe the type of charge carriers, number of bands crossing the Fermi level as well as the presence of hole pockets once suitable single crystals become available[14].

## III. EXPERIMENTS

Polycrystalline $Ce_3Pd_{20}X_6$ ($X$ = Si, Ge) samples were prepared by arc-melting stoichiometric mixtures of the pure elements (Ce:3N; Pd:3N; Si:10N; Ge:5N) in an argon

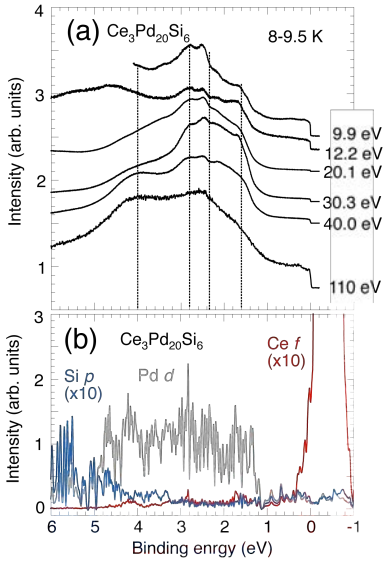


FIG. 6. (Color online). (a) Valence-band spectra near the Fermi edge at 8−9.5 K and $h\nu = 9.9$, 12.2, 20.1, 30.3, 40 and 110 eV for $Ce_3Pd_{20}Si_6$. (b) Partial density of states calculated within DFT for $Ce_3Pd_{20}Si_6$.

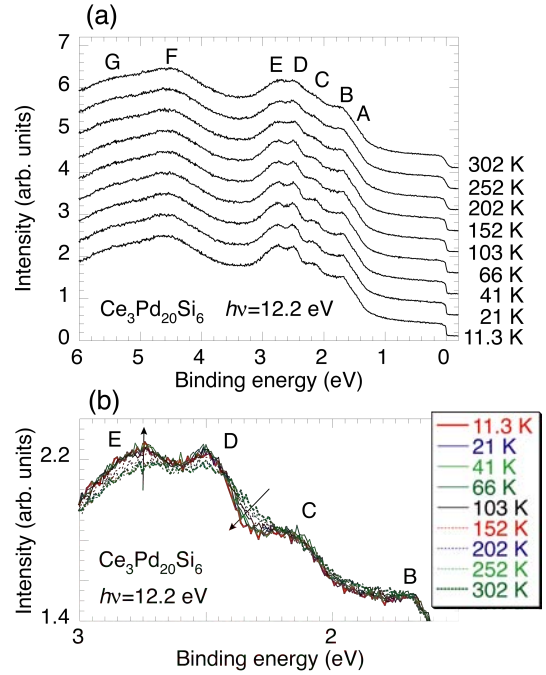


FIG. 7. (Color online). (a) Temperature dependence of the valence-band spectra at $h\nu = 12.2$ eV for $Ce_3Pd_{20}Si_6$. (b) Enlarged view of the valence-band spectra in (a) near the Fermi edge. Direction of arrow corresponds to change in the intensity at given binding energy when temperature decreases.

gas atmosphere and subsequent annealing in an evacuated quartz tube for 120 hours at 800 °C.[21] The annealed samples were examined by powder x-ray diffraction and found to be single phased.

SX and UV PES measurements were performed at the undulator beamlines BL-1 and BL-9A at the Hiroshima Synchrotron Radiation Center HiSOR, equipped with high-resolution hemispherical electron-energy analyzers (R4000, VG-SCIENTA).[37,38] In the UV PES the total energy resolution ($\Delta E$) was set to be less than 20 meV at $h\nu$ = 10-20 eV and 9 K under the vacuum pressure below $2\times10^{-9}$ Pa. In the SX PES $\Delta E$ was less than 50 meV for $h\nu = 122$ eV and 10 K with a vacuum pressure below $10^{-8}$ Pa. The energy resolution and the Fermi level, used for the binding energy calibration, are determined by fitting the Fermi edge of polycrystalline Au evaporated on the sample holders using a convolution of a Gaussian and the Fermi-Dirac function. All samples were fractured at a temperature of around 10 K in-situ just before the measurements.

In these compounds there are two Ce sites, which are expected to show different physical properties and temperature behavior. Our photoemission experiment, however, averages over both Ce sites.

## IV. EXPERIMENTAL RESULTS AND DISCUSSION

### A. Temperature dependence

Figure 6 shows valence-band spectra in the wide binding energy range at 8−9.5 K and several incident photon energies for $Ce_3Pd_{20}Si_6$. As shown in the DFT calculations, in these spectra we observe the contribution from mainly Pd 4$d$ DOS and partially Si 3$p$ DOS. The electronic structure in this energy range below the 4$d$-4$f$ resonance reflects the Pd 4$d$ DOS because of the low photoionization cross-section of 4$f$ electrons.[39] The Pd 4$d$ contribution to the valence band mainly consists of three peaks at $E_b \sim 1.6$ eV, ∼2.5 eV, and ∼ 4 eV. The Pd 4$d$ peak at $E_b \sim 2.5$ eV at $h\nu = 110$ eV splits into fine peaks at $E_b < 40$ eV because of the better resolution in the UV range. The intensity at $E_b > 5$ eV in Fig. 6(a) increases at $h\nu = 12.2$ eV due to the increase of the Si 3$p$ photoionization cross-section.[39] The DFT calculation in Fig. 6(b) corresponds well to the $h\nu$-dependent PES spectra. They mainly reflect the contribution from Pd 4$d$ states due to the low cross sections for Ce 4$f$ and Si 3$p$ states.

Temperature dependence of the valence-band spectrum of $Ce_3Pd_{20}Si_6$ at $h\nu = 12.2$ eV is shown in Fig. 7. The intensity is normalized by the area at $E_b < 8.2$ eV.

This incident photon energy is more bulk sensitive compared to the Ce $4d$-$4f$ resonance energy and thus the surface contribution is reduced. The valence-band spectra mainly reflect the Pd $4d$ and Si $3p$ DOS. Figure 7(b) shows that the peaks E and D becomes sharper with decreasing temperature. This may be caused by the suppression of thermal broadening at low temperatures or a narrowing of the band width in the valence band caused by increased electronic localization. The temperature dependence of the Fermi edge, at low photon energies, can be explained reasonably well by the Fermi-Dirac distribution function. These results indicate a very weak temperature dependence of the Pd $4d$ states.

Figure 8 shows temperature dependence of the valence-band spectra at $h\nu = 122$ eV, where Ce $4d$-$4f$ resonance occurs. Based on the analogy to the $CePd_3$ spectra[40,41] we assign the two sharp peaks near the Fermi edge and the broad peak around 1.4−1.6 eV to Ce $4f^1{}_{5/2}$, $4f^1{}_{7/2}$ (spin-orbit satellite), and $4f^0$, respectively. The broad maximum peak around 1.4−1.6 eV may include a tail of the surface contribution of the Ce $4f$ components as well as that of the Pd $4d$ components.[41,42] We can confirm these assignments of the $4f$ peaks in the incident energy dependence of the $4d$-$4f$ resonance spectra described below because of the resonant intensity enhancement of these peaks.

We observe a strong $f^0$ weight with a weak $f^1$ weight in the valence-band spectra, indicating weak $c$-$f$ hybridization, and localized nature of Ce $4f$ electrons. In Ce system it undergoes from the Kondo regime to the mixed valence regime with the hybridization strength.[43] For the PES spectrum the Anderson impurity model (AIM) predicts the coherent sharp peak (Kondo resonance) at $k_{\rm B}T_{\rm K}$ ($T_{\rm K}$: Kondo temperature) above $E_{\rm F}$ and the tail of the Kondo peak should be observed just below the Fermi edge with incoherent broad side bands of $f^0$ as a consequence of the $c$-$f$ hybridization. These features are intrinsically many body characters. It is normally considered that $4f^0$ is the final sate with localized or poorly-screened $4f$ character and $4f^1{}_{5/2}$ final state is forming the tails of the Kondo resonance with itinerant or well-screened character. The $4d$-$4f$ resonant spectra of $Ce_3Pd_{20}Si_6$ can be explained by the framework of the AIM. Here we note that in $CePd_3$ the Ce $3d$ core-level spectrum showed a relatively weak $f^0$ component compared to the intensity of $f^1$ and $f^2$.[40] This was considered a rather accurate indicator of the hybridization in the ground state. Actually the magnetic susceptibility measurement showed Ce charge state of nearly 3+.[1] The core-level spectroscopy of Ce $3d$ for for $Ce_3Pd_{20}X_6$ is also desired to obtain the exact valence state in the ground state.

In Fig. 8(a) the spectral weight of the Pd $4d$ component at $E_{\rm b} \sim 2.5$ eV seems to decrease with decreasing temperature similar to what we have shown for low photon energies (compare Figs. 7(a) and 7(b)). However here the feature lies on the tail of a strong $f^0$ component and may overlap with the $4f$ surface contribution. Therefore the low photon energy measurement give more reliable information about the temperature dependence of the Pd $4d$ dominated valence band.

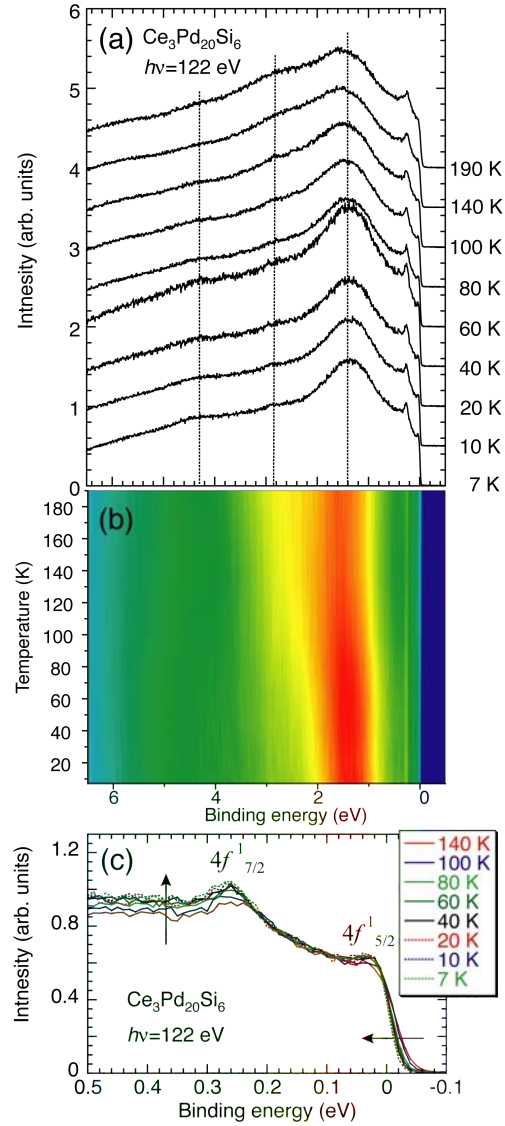


FIG. 8. (Color online). (a) Temperature dependence of the valence-band spectra at $h\nu = 122$ eV for $Ce_3Pd_{20}Si_6$. (b) Contour intensity map of temperature dependence of the valence-band spectra in (a). (c) Enlarged view of the valence-band spectra in (a) near the Fermi edge. Direction of arrows in (c) correspond to change in the intensity at given binding energy when temperature decreases.

In Fig. 8(c) an expanded view of the valence-band spectra near $E_{\rm F}$ is shown as a function of temperature. We observe a peak at $E_{\rm b} \sim 0.28$ eV, which reflects the Ce $4f_{7/2}$ spectral feature. The temperature dependence of the resistivity showed the onset of the Kondo screening with a maximum at about 20 K.[8] We should observe the development of the psudogap around the Fermi edge at low temperatures due to the hybridization.[1,13] However, the intensity of $4f_{5/2}$ in Fig. 8(c) only shows a weak

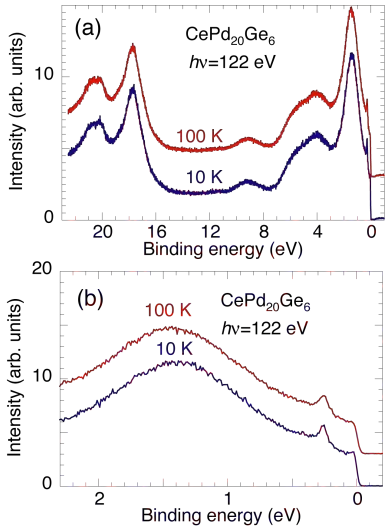


FIG. 9. (Color online). (a) Valence-band spectra at 10 and 100 K at $h\nu = 122$ eV for $Ce_3Pd_{20}Ge_6$. (b) Enlarged view of the valence-band spectra in (a) near the Fermi edge.

temperature dependence because of the resolution broadening of 40 meV. Winkler *et al.*[6,7] concluded that the Ce ions at (4a) site plays a minor role in the incoherent Kondo scattering at high temperatures and Ce ions at the (8c) site have a higher Kondo temperature than those at the (4a) site. Our PES is not cite-selective and thus indicates a superposition of the valence-band spectra from the two distinct Ce sites. High-resolution angle resolves photoemission spectroscopy measurements of the valence-band spectra from single crystals remain future work.

In Figs. 9(a) and 9(b) we show the valence-band spectra of $Ce_3Pd_{20}Ge_6$ at 10 and 100 K. We do not see significant temperature dependence. This result is reasonable because the Kondo temperature was estimated to be on the order of a few K,[2] which is below the temperature measured in this experiment.

### B. Resonant PES

Figures 10(a) and 10(b) show the valence-band spectra measured around $h\nu = 110 - 130$ eV for $Ce_3Pd_{20}Si_6$ and $Ce_3Pd_{20}Ge_6$, respectively, where the Ce $4d$-$4f$ resonance occurs. In Figs. 10(c) and 10(d) we show contour intensity maps as a function of the incident photon energies, where a strong enhancement of the intensity of $4f^1$ and $4f^0$ components is observed at the $4d$-$4f$ resonance. This again confirms the assignment of these $4f$ components described above. Pd $4d$ state has a Cooper minimum at around $h\nu \sim 115$ eV.[39] The cross section of the Ce $4f$ state is actually decreasing above $h\nu \sim 60$ eV.

In Fig. 10(e) we show the spectra of on- and off-resonance for $Ce_3Pd_{20}Si_6$ and $Ce_3Pd_{20}Ge_6$. Figure 10(f)

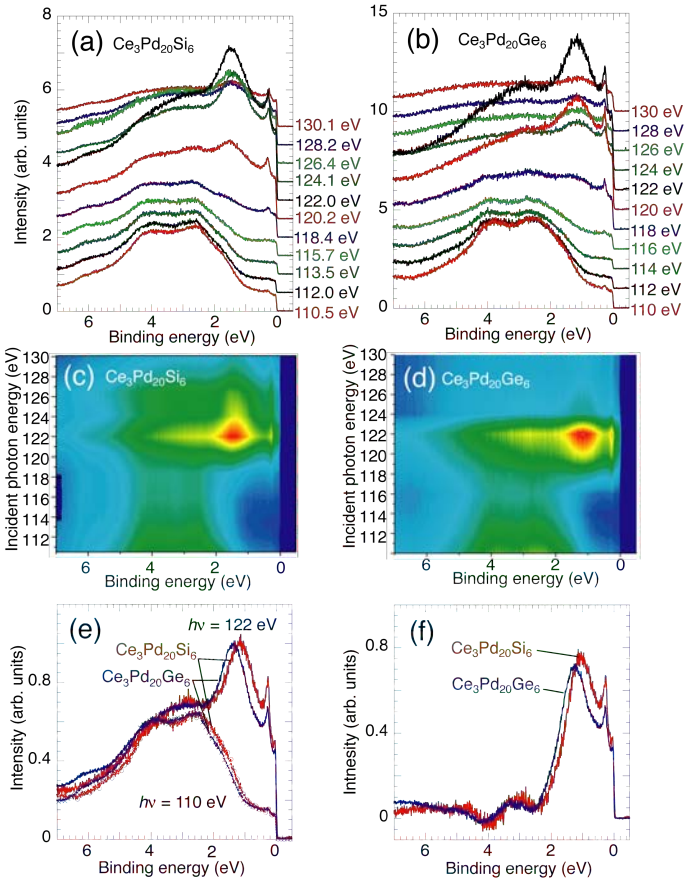


FIG. 10. (Color online). (a) Resonant photoelectron spectra of valence band for $Ce_3Pd_{20}Si_6$ at 8 K in the incident energy range of $h\nu = 110.5$-$130.1$ eV. (b) Contour intensity map of the resonant spectra in (a) as a function of the incident photon energies. (c) Resonant photoelectron spectra of valence band for $Ce_3Pd_{20}Ge_6$ at 10 K in the incident energy range of $h\nu = 110$-$130$ eV. (d) Contour intensity map of the resonant spectra in (c) as a function of the incident photon energies. (e) Comparison of the spectra at 110 eV (off resonance) and 122 eV (on resonance) for $Ce_3Pd_{20}Si_6$ and $Ce_3Pd_{20}Ge_6$. The on-resonance spectra are normalized at 7 eV. The off-resonant spectra intensity is normalized to the intensity at 4 eV for the on-resonance spectra. (f) Difference of the intensity between on and off resonant spectra for $Ce_3Pd_{20}Si_6$ and $Ce_3Pd_{20}Ge_6$.

shows the intensity difference between the spectra on- and off-resonance. The off-resonant spectra do not show a significant difference between these two compounds. We should note, however, that the relative spectral intensity ratio $f^1/f^0$ for $Ce_3Pd_{20}Si_6$ is apparently stronger than that for $Ce_3Pd_{20}Ge_6$. This result indicates that the $c$-$f$ hybridization of $Ce_3Pd_{20}Si_6$, even though weak compared to other correlated materials, is stronger than that of $Ce_3Pd_{20}Ge_6$ and this is a possible origin of the larger $\gamma$ of $Ce_3Pd_{20}Si_6$.

In the DFT calculations no pronounced difference is observed in the valence and conduction bands between $Ce_3Pd_{20}Si_6$ and $Ce_3Pd_{20}Ge_6$ although the band struc-

ture close to $E_F$ is different. In general, photoemission spectra are described by single-particle spectral function, which is in proportion to the imaginary part of the single-particle Greens function.[44] Especially, in the case of the Ce $4f$ derived spectra, due to strong electron correlation, the self-energy correction plays an important role. Thus the Ce $4f$ spectrum deviates significantly from the DOS predicted by the DFT calculation for the ground state electronic structure. For the angle-integrated Ce $4f$ spectra, we assume that AIM can describe the observed major spectral features. However, in order to analyze the Ce $4f$ spectra quantitatively, we would need to separate the electronic states at (8c) and (4a) sites as well as surface contribution.

## V. CONCLUSION

We performed detailed density functional theory calculations and high-resolution photoelectron spectroscopy measurements for the heavy fermion compound $Ce_3Pd_{20}X_6$ ($X$ = Si, Ge) in the UV and SX photon energy ranges and we were able to clarified both experimentally and theoretically the different contributions to the electronic structure.

The DFT calculation of the density of states was able to identify the main orbital contributions to the valence band and conduction band of these materials and shows an overall good agreement with the experimental valence-band spectra. By comparing calculated and experimental values of the electronic specific heat coefficient $\gamma$ we were able to gauge the relative strength of correlation in both compounds. Even though the calculation was not able to describe electron correlations, the presence of $c$-$f$ hybridization was supported by comparing a plot of the $d$ and $f$ weights in the $k$-dependent band structure. At the Fermi level, differences in the band structures of $Ce_3Pd_{20}Si_6$ and $Ce_3Pd_{20}Ge_6$ could be shown to exist and strongly motivate future experiments.

Experimentally we demonstrated that the valence-band spectra of $Ce_3Pd_{20}Si_6$, taken at low photon energies, show only a weak temperature dependence and are dominated by Pd $d$ states. Tuning the photon energies across the Ce $4d$-$4f$ resonance, in the soft x-ray regime, clearly revealed Ce $4f$ states in the valence band close to $E_F$ of these compounds. However, even at resonance no pronounced temperature dependence was observed in the valence band or at $E_F$ of these compounds. We further observe a rather strong $f^0$ ($Ce^{4+}$) component with only a small fraction of $f^1$ ($Ce^{3+}$) component, indicating weak $c$-$f$ hybridization and a more localized nature of the $4f$ electrons in these correlated materials. The relative intensity $f^1/f^0$ for $Ce_3Pd_{20}Si_6$ is stronger than that of $Ce_3Pd_{20}Ge_6$ at $4d$-$4f$ resonance, suggesting stronger $c$-$f$ hybridization in the former. This may hint to the origin of the large electronic specific heat coefficient of $Ce_3Pd_{20}Si_6$. In order to detect Kondo-like behavior near $E_F$, high-resolution low temperature photoemission measurements of the electronic structure should be performed.

## ACKNOWLEDGMENTS

The experiments were performed at HiSOR beamlines BL-1 and BL-9A (HiSOR under Proposals No. 11-A-10 & No. 12-A-1) in Hiroshima University. We thank the N-BARD, Hiroshima University for supplying the liquid helium as well as P. Aebi for helpful discussion. E. F. S acknowledges financial support by the JSPS postdoctoral fellowship for overseas researchers as well as the Alexander von Humboldt Foundation and the Swiss National Foundation fellowship for prospective researchers (grant number: PBFRP2_140028)

* Corresponding author: yamaoka@spring8.or.jp
† Corresponding author: schwier@hiroshima-u.ac.jp

[1] N. Takeda, J. Kitagawa, and M. Ishikawa, J. Phys. Soc. Jpn. **64**, 387 (1995).
[2] J. Kitagawa, N. Takeda, and M. Ishikawa, Phys. Rev. B **53**, 5101 (1996).
[3] A. M. Strydom, A. Pikul, F. Steglich, and S. Paschen, J. Phys.: Conf. Ser. **51**, 239 (2006).
[4] S. Paschen, M. Müller, J. Custers, M. Kriegisch, A. Prokofiev, G. Hilscher, W. Steiner, A. Pikul, F. Steglich, and A. M. Strydom, J. Magn. Magn. Mater. **316**, 90 (2007).
[5] A. Prokofiev, J. Custers, M. Kriegisch, S. Laumann, M. Müller, H. Sassik, R. Svagera, M. Waas, K. Neumaier, A. M. Strydom, and S. Paschen, Phys. Rev. B **80**, 235107 (2009).
[6] H. Winkler, S. Laumann, J. Custers, A. Prokofiev, and S. Paschen, Phys. Status Solidi B **247**, 516 (2010).
[7] H. Winkler, K.-A. Lorenzer, S. Laumann, J. Custers, A. Prokofiev, and S. Paschen, J. Phys.: Condens. Matter **23**, 094208 (2011).
[8] J. Custers, K.-A. Lorenzer, M. Müller, A. Prokofiev, A. Sidorenko, H.Winkler, A. M. Strydom, Y. Shimura, T. Sakakibara, R. Yu, Q. Si, and S. Paschen, Nature Mater. **11**, 189 (2012).
[9] A. Prokofiev, A. Sidorenko, K. Hradil, M. Ikeda, R. Svagera, M. Waas, H. Winkler, K. Neumaier, and S. Paschen, Nature Mater. **12**, 1096 (2013).
[10] A. V. Grivanov, Yu. D. Seropegin, and O. I. Bodak, J. Alloys & Compd. **204**, L9 (1994).
[11] T. Goto, T. Watanabe, S. Tsuduki, H. Kobayashi, Y. Nemoto, T. Yanagisawa, M. Alatsu, G. Ano, O. Suzuki, N. Takeda, A. Dönni, and H. Kitazawa, J. Phys. Soc. Jpn. **78**, 024716 (2009).
[12] H. Mitamura, T. Tayama, T. Sakakibara, S. Tsuduki, G. Ano, I. Ishii, M. Akatsu, Y. Nemoto, T. Goto, A. Kikkawa, and H. Kitazawa, J. Phys. Soc. Jpn. **79**, 074712 (2010).
[13] Yu. P. Gaĭdukov, Yu. A. Koksharov, Yu. V. Kochetkov,

I. Mirkovich, and V. N. Nikiforov, JETP Lett. **61**, 391 (1995).
[14] P. Y. Portnichenko, A. S. Cameron, M. A. Surmach, P. P. Deen, S. Paschen, A. Prokofiev, J. M. Mignot, A. M. Strydom, M. T. F. Telling, A. Podlesnyak, and D. S. Inosov arXiv.org, 1410.0296v1 (2014).
[15] H. Ono, T. Nakano, N. Takeda, G. Ano, M. Akatsu, Y. Nemoto, T. Goto, and H. Kitazawa, J. Phys.: Conf. Ser. **391**, 012054 (2012).
[16] H. Ono, T. Nakano, N. Takeda, G. Ano, M. Akatsu, Y. Nemoto, T. Goto, A. Dönni, and H. Kitazawa, J. Phys.: Condens. Matter **25**, 126003 (2013).
[17] S. Paschen and J. Larrea, J. Phys. Soc. Jpn. **83**, 061004 (2014).
[18] J. Custers, P. Gegenwart, C. Geibel, F. Steglich, P. Coleman, and S. Paschen, Phys. Rev. Lett. **104**, 186402 (2010).
[19] T. Hashiguchi, N. Takeda, J. Kitagawa, N. Wada, S. Takayanagi, M. Ishikawa, and N. Mori, J. Phys. Soc. Jpn. **69**, 667 (2000).
[20] P. P. Deen, A. M. Strydom, S. Paschen, D. T. Adroja, W. Kockelmann, and S. Rols, Phys. Rev. B **81**, 064427 (2010).
[21] A. Dönni, H. Kitazawa, T. Strässle, L. Keller, M. Matsuda, K. Kakurai, G. Ano, M. Akatsu, Y. Nemoto, and T. Goto, J. Phys. Soc. Jpn. **80**, 044715 (2011).
[22] A. Dönni, T. Hermannsdörfer, P. Fischer, L. Keller, F. Fauth, K. A. McEwen, T. Goto, and T. Komatsubara, J. Phys.: Condes. Matter **12**, 9441 (2000).
[23] V. N. Duginov, K. I. Gritsaj, V. Yu. Pomjakushin, A. N. Ponomarev, A. A. Nezhivoy, A. V. Gribanov, V. N. Nikiforov, and Yu. D. Seropegin, Physica (Amsterdam) **374-375B**, 192 (2006).
[24] H. Harima, Physica (Amsterdam) **281 & 282 B**, 775 (2000).
[25] T. Yamamizu, M. Nakayama, N. Kimura, T. Komatsubara, and H. Aoki, Physica (Amsterdam) **312-313B**, 495 (2002).
[26] Y. Nemoto, T. Yamaguchi, T. Horino, M. Akatsu, T. Yanagisawa, T. Goto, O. Suzuki, A. Dönni, and T. Komatsubara, Phys. Rev. B **68**, 184109 (2003).
[27] T. Watanabe, T. Yamaguchi, Y. Nemoto, T. Goto, N. Takeda, O. Suzuki, and H. Kitazawa, J. Magn. Magn. Mater. **310**, 280 (2007).
[28] H. Yamaoka, P. Thunström, I. Jarrige, K. Shimada, N. Tsujii, M. Arita, H. Iwasawa, H. Hayashi, J. Jiang, T. Habuchi, D. Hirayama, H. Namatame, M. Taniguchi, U. Murao, S. Hosoya, A. Tamaki, and H. Kitazawa, Phys. Rev. B **85**, 115120 (2012).
[29] H. Yamaoka, P. Thunström, N. Tsujii, I. Jarrige, K. Shimada, M. Arita, H. Iwasawa, H. Hayashi, J. Jiang, H. Namatame, M. Taniguchi, N. Hiraoka, H. Ishii, K.-D. Tsuei, M. Giovannini, and E. Bauer, Phys. Rev. B **86**, 085137 (2012).
[30] http://elk.sourceforge.net/
[31] J. P. Perdew and Y. Wang, Phys. Rev. B **45**, 13244 (1992).
[32] H. J. Monkhorst and J. D. Pack, Phys. Rev. B **13**, 5188 (1976).
[33] *elk* user manual
[34] Note that similar to Fig. 2 the spin and site resolved partial density of states is obtained by summing over the DOS of equivalent atoms in the unit cell.
[35] The image plot is obtained by calculating the $d$ and $f$ weight inside the muffin-tin of each Pd and Ce site at each $k$-point along the high symmetry path and adding a gaussian function with $\sigma = 75$ meV with an area corresponding to the $d$ and $f$ weights centered at the eigenenergy of the band.
[36] If we use a typical approximation for the width of the Fermi Dirac distribution to be $\sim 5k_BT$ and assume the least favorable Fermi level position, situated exactly in between both bands, then electrons or holes from the bands could be thermally excited across the Fermi level at temperatures of $\sim 8$ K due to the presence of other bands crossing the Fermi level.
[37] K. Shimada, M. Arita, Y. Takeda, H. Fujino, K. Kobayashi, T. Narimura, H. Namatame, and M. Taniguchi, Surf. Rev. & Lett. **9**, 529 (2002).
[38] M. Arita, K. Shimada, Y. Takeda, M. Nakatake, H. Namatame, and M. Taniguchi, Surf. Rev. & Lett. **9**, 535 (2002).
[39] J. J. Yeh and I. Lindau, At. Data Nucl. Data Tables **32**, 1 (1985).
[40] M. Zacchigna, J. Almeida, I. Voboronik, G. Margaritondo, D. Malterre, B. Malaman, and M. Grioni, Eur. J. Phys. **2**, 463 (1998).
[41] S. Danzenbächer, Yu. Kucherenko, M. Heber, D. V. Vyalikh, S. L. Molodtsov, V. D. P. Servedio, and C. Laubschat, Phys. Rev. B **72**, 033104 (2005).
[42] M. Mulazzi, K. Shimada, J. Jiang, H. Iwasawa, and F. Reinert, Phys. Rev. B **89**, 205134 (2014).
[43] H. Yamaoka, I. Jarrige, N. Tsujii, A. Kotani, J.-F. Lin, F. Honda, R. Settai, Y. Ōnuki, N. Hiraoka, H. Ishii, and K.-D. Tsuei, J. Phys. Soc. Jpn. **80**, 124701 (2011).
[44] G. Borstel, Appl. Phys. A **38**, 193 (1985).